Simulated extratropical responses to Amazon deforestation

David Medvigy[a], Robert L. Walko[b], Martin J. Otte[c], and Roni Avissar[b]

[a]Department of Geosciences and Program in Atmospheric and Oceanic Sciences, Princeton University, Princeton, NJ

[b]Rosenstiel School of Marine and Atmospheric Science, University of Miami, Miami, FL

[c]Atmospheric Modeling and Analysis Division, US Environmental Protection Agency, Research Triangle Park, NC

Corresponding Author:
David Medvigy
Princeton University, Department of Geosciences
418B-Guyot Hall
Princeton, NJ 08544
USA
Phone: 1-609-258-9017
Email: dmedvigy@princeton.edu

ABSTRACT

Numerical models have long predicted that the deforestation of the Amazon would lead to large regional changes in precipitation and temperature, but the extratropical effects of deforestation have been a matter of controversy. Here, the simulated impacts of deforestation on Northwest United States December-January-February climate are investigated. Integrations are carried out using the Ocean-Land-Atmosphere Model (OLAM), here run as a variable-resolution atmospheric GCM, configured with three alternative grid meshes: (1) 25 km characteristic length scale (CLS) over the US, 50 km CLS over the Andes and Amazon, and 200 km CLS in the far-field; (2) 50 km CLS over the US, 50 km CLS over the Andes and Amazon, and 200 km CLS in the far-field; (3) 200 km CLS globally. In the high-resolution simulations, Amazon deforestation results in 10-20% precipitation reductions for the coastal Northwest US and the Sierra Nevada. Snowpack in the Sierra Nevada experiences declines of up to 50%. These changes are associated with a modification of the jet stream such that storms are diverted away from the Northwest US and most of California. However, in the coarse-resolution simulations, this modification to the jet stream does not occur, and precipitation is not reduced in the Northwest US. These results highlight the need for adequate model resolution in modeling the impacts of Amazon deforestation. We conclude that the deforestation of the Amazon can act as a driver of regional climate change in the extratropics, including areas of the western US that are agriculturally important.

1. Introduction

Many numerical models have predicted that Amazon deforestation would lead to local increases in surface temperature and decreases in precipitation (Henderson-Sellers et al. 1993; Lean and Rowntree 1993; Gash and Nobre 1997; Hahmann and Dickinson 1997; Costa and Foley 2000; Gedney and Valdes 2000; Werth and Avissar 2002; Avissar and Werth 2005; Findell et al. 2006; Sampaio et al. 2007; Hasler et al. 2009; Medvigy et al. 2011). However, deforestation is likely to have other complex effects on climate. For example, the fires that frequently accompany deforestation affect aerosol concentrations, reduce cloud droplet size, and can intensify updrafts (Williams et al. 2002; Andreae et al. 2004). Such changes can increase the vigor of individual convective events even if annual average rainfall decreases. It has also been proposed, not without controversy, that Amazon deforestation can impact extratropical climate (Gedney and Valdes 2000; Werth and Avissar 2002; Findell 2006; Medvigy et al. 2012). These studies of extratropical impacts have all relied on numerical models, and thus are subject to all the caveats that are generally associated with model simulations. Using observations to directly assess extratropical impacts of deforestation is extremely difficult because large-scale deforestation has only been going on for a few decades and thus any signal would be obscured by natural climate variability. Furthermore, total deforested area in the Amazon may increase by a factor of 2-3 in the next few decades to 40-60% (Soares-Filho et al. 2006; Walker et al. 2009), and this may lead to a very different climatic response than that arising from the pattern of deforestation that exists today (Ramos da Silva et al. 2008).

It is possible that other climate anomalies can be used to better understand the impacts of Amazon deforestation. El Niño events, for example, arise from the natural variability of tropical climate. El Niño operates by bringing increased near-surface temperatures and increased convective activity to the eastern tropical Pacific. This results in the strengthening and contraction of the Hadley cell, and an equatorward shift of the tropospheric zonal jets (Seager et al. 2003, 2005). Midlatitudes are affected by changes in transient-eddy momentum fluxes and in the eddy-driven mean meridional circulation that result from changes in the jet (Seager et al. 2005). The northwest US, including northern California and western Oregon and Washington, is affected particularly strongly. Composite maps show an intensified Aleutian low and ridging high pressure in the Pacific Northwest, which results in warm, dry weather in this sector (Ropelewski and Halpert 1987, 1989; Redmond and Koch 1991; Wallace et al. 1992; Cayan 1996). This warm and dry anomaly has important societal and ecological implications, affecting drought, snowpack, and fires (Dai et al. 1998; Enfield et al. 2001; McCabe et al. 2004; Seager et al. 2010).

It has previously been suggested that Amazon deforestation may generate an extratropical signature that resembles the extratropical signature of El Niño (Avissar and Werth 2005). For example, El Niño brings increased near-surface temperatures and increased convective activity to the eastern tropical Pacific, and Amazon deforestation is likely to bring increased temperatures and increased convective activity to tropical South America. Of course, Amazon deforestation and El Niño differ in important ways, including the obvious fact that the Amazon is situated to the east and somewhat to the south of the eastern tropical Pacific. However, different historical El Niño events having large differences in equatorial SST anomalies have nonetheless elicited quite similar extratropical responses (Hoerling and Ting 1994). Thus, we conjecture here that there will be important similarities between the extratropical responses to El Niño and to Amazon deforestation. In particular, this study will focus on the northwest US because this region is known to be highly sensitive to El Niño.

Analysis of this problem in the context of numerical models is difficult. Many climate models give large underestimates of the climatological precipitation in the Amazon (Randall et al. 2007), and it is uncertain if this would compromise their ability to simulate the impacts of Amazon deforestation. In one recent study, it was shown that simulation of the Amazon hydroclimate markedly improved when model resolution of the Andes became finer, and that the model failed to capture interannual variability of precipitation in the Amazon until the Andes were simulated at < 100 km resolution (Medvigy et al. 2008). Furthermore, in the US, the impacts of El Niño are highly regional, and may be challenging to resolve with current GCMs. Previous work has shown that adequate resolution of topography is critical for correctly simulating precipitation in the northwest US (Leung and Qian 2003; Leung et al. 2003a,b; Zhang et al. 2012). Leung et al. (2003a,b) carried out sensitivity analyses and found that a 40 km resolution was adequate for simulating seasonal and interannual precipitation variability in the region. Leung and Qian (2003) compared simulations at 40 km and 13 km, and found that simulation of snowpack was greatly improved at the higher resolution, but differences in precipitation biases were small.

The computational problem of carrying out high-resolution simulations becomes more tractable by using a variable-resolution GCM. Variable-resolution GCMs allow for fine resolution in the region of interest with a coarser, more computationally efficient resolution in the far-field. This enables the simulation of regional-scale circulations without the need for lateral boundary conditions, while maintaining a reasonable computational cost (Medvigy et al. 2008, 2010, 2011). In this study, we use the Ocean-Land-Atmosphere Model (OLAM) (Walko and Avissar 2008a,b, 2011) variable-resolution GCM to investigate the impacts of Amazon deforestation on the US. Unlike past studies, we use locally fine-resolution grid spacing over both North America and South America. Because El Niño has particularly large effects over the US during winter (e.g., Harrison and Larkin 1998), by analogy our focus is on the December-January-February (DJF) season. The objectives of this work are to identify impacts of Amazon deforestation on the US during DJF, identify relevant mechanisms, and assess the sensitivity of the mechanisms to model resolution.

2. Model simulations

We used the OLAM model (Walko and Avissar 2008a,b, 2011) run as an atmospheric GCM with prescribed sea-surface temperatures (SSTs). Amazon deforestation has previously been simulated with OLAM (Medvigy et al. 2011, 2012), and the model's ability to simulate global and especially South American precipitation, temperature, and surface solar radiation has previously been evaluated (Medvigy et al. 2008, 2010, 2011, 2012). In this study, we carried out multiple pairs of simulations. The pairs of simulations differed only in their grid mesh. In our first pair ("FINE"), the grid mesh had a 50 km characteristic length scale (CLS) over the Andes, most of the Amazon, and also over the contiguous US (Fig. 1a,b). This 50 km CLS was previously shown to be adequate for OLAM to simulate South American hydroclimate (Medvigy et al. 2008).

The grid mesh gradually expanded to 200 km away from North and South America. Second, we carried out a pair of simulations with the same horizontal grid mesh as FINE, but with enhanced vertical resolution ("FINEV"; see below). Third, we carried out a pair of simulations with the same vertical resolution as FINE but with a more refined horizontal mesh. This pair, "XFINE", had a 50 km CLS over the Andes and most of the Amazon and a 25 km CLS over most of the contiguous US (Fig. 1c). The purpose of the FINEV and XFINE pairs was to evaluate and challenge the conclusions stemming from the FINE pair. Finally, we carried out a coarse pair of simulations ("COARSE"), in which the entire globe was simulated with a uniform 200 km CLS, which is a typical GCM resolution (Fig. 1d). This pair would be most comparable to previous investigations of the extratropical impacts of Amazon deforestation.

The FINE, XFINE, and COARSE simulations used a Cartesian vertical grid consisting of 53 levels, with the grid spacing stretching from 200 m near the surface to 2 km near the model top at 45 km. The FINEV simulations also used a Cartesian vertical grid, but in this case there were 74 levels, with the grid spacing stretching from 100 m near the surface to 2 km near the model top at 45 km. As a post-processing step, upper-air variables were interpolated to pressure levels. For the convective parameterization, we used the Eta version of the Kain-Fritsch scheme (Kain 2004), which has been shown to work well in variable-resolution OLAM runs (Kim et al., in prep.). All other parameterizations are the same as those used in Medvigy et al. (2011).

In each pair, the two pair members correspond to two land cover scenarios, tagged as forested ("FOR") and deforested ("DEF"). These land cover scenarios are described in detail in Medvigy et al. (2011) and are only briefly described here. In our FOR runs, each land grid cell is assigned a single land cover classification according to the Olson Global Ecosystem framework (Olson 1994a,b), which was based on satellite imagery from 1992-93. About 10% of the Amazon sector is classified as agriculture or short grass in FOR. Our corresponding DEF runs are identical to the corresponding FOR runs in every way except land cover classification. The DEF runs, meant to represent the total deforestation of the Amazon, classes all land grid cells between 75-49°W and 15-0°S (boxed areas in Fig. 1) as deforested land cover. The land surface and vegetation properties of these deforested grid cells are prescribed according to in situ measurements at pasture sites (Gash and Nobre 1997) and have been tested in previous studies (Gandu et al. 2004; Avissar and Werth 2005; Ramos da Silva et al. 2008; Hasler et al. 2009; Medvigy et al. 2011). A more sophisticated treatment might distinguish between pasture, soy, and cultivation of other crops, but we expect differences between these types to be much smaller than the differences between tropical forest and pasture (Sampaio et al. 2007). The naming convention that we use for our simulations combines the grid mesh identifier (FINE, FINEV, XFINE, or COARSE) with the land cover identifier (FOR or DEF), e.g., FINE-FOR. Our simulations are summarized in Table 1.

Atmospheric and soil initial conditions were prescribed from NCEP reanalysis from October 1, 1996, 0000 UTC (Kalnay et al. 1996). All simulations were forced with weekly, 1° sea-surface temperatures (SSTs) (Reynolds et al. 2002), and sea ice extent from NCEP reanalysis (Kalnay et al. 1996). CO_2 and other greenhouse gas concentrations were held fixed throughout all the simulations at current-day levels to enable us to isolate the effects of deforestation. We simulated the period from October 1, 1996 to April 1, 2012. Preliminary simulations using climatological SSTs indicated that soil moisture and soil temperature in the Amazon region equilibrate after about a year, and so all days prior to March 1, 1998 were discarded as spin-up, leaving 14 years for analysis. In this paper, we limited our analysis to December-January-February (DJF), though the other months were saved to disk and are available for future analyses.

We performed a series of statistical tests to evaluate the significance of differences between the DEF and FOR simulations. The 95% confidence level is taken as the threshold for statistical significance throughout this paper. Tests were performed for each pair (FINE, FINEV, XFINE, or COARSE) by itself, as well as for the ensemble consisting of the FINE, FINEV, and the XFINE pairs (note that the COARSE pair was excluded, for reasons that will become evident later). All statistical tests are conducted in R (R Development Core Team 2008). A *t*-test can be used to test the null hypothesis that the means from the DEF and FOR simulations are equal, provided that the DEF and FOR samples are independent and normally distributed. If the normality assumption does not hold, a non-parametric test such as the Wilcoxon signed-rank test ("wilcox.test" in R; Hollander and Wolfe 1999) may be used instead of the *t*-test. The null hypothesis of the Wilcoxon signed-rank test is that the median difference between the DEF and FOR samples is zero. We used the Shapiro-Wilk test ("shapiro.test" in R; Royston 1982) to test for normality. We occasionally found that the normality assumption was violated for as many as 15-20% of the grid cells, and so we conservatively adopted the Wilcoxon signed-rank test as our test of choice in this paper. We used the Ljung-Box test ("Box.test" in R; Ljung and Box 1973) to test for independence. In no case did we find that the assumption of independence was violated for more than 5% of the grid cells, and so we adopted independence as a generally reasonable assumption.

3. Results

a. Model evaluation for North America

We limited our model evaluation to North America because model evaluation for South America has already been carried out (Medvigy et al. 2008, 2010, 2011, 2012). Precipitation and near-surface temperature are evaluated using the Princeton Global Forcings (PGF) dataset at 0.5° resolution (Sheffield et al. 2006). This dataset blends surface observations with reanalysis and is available for 1948-2008. Because this study focuses on DJF quantities and our (post-spin-up) simulations begin in March 1998, we defined a climatological winter daily precipitation rate and daily temperature by averaging the daily values of these quantities over all days in December, January, and February within the period March 1998 through December 2008. We constructed such climatological averages for our FINE-FOR, FINEV-FOR, XFINE-FOR, and COARSE-FOR simulations.

The PGF precipitation dataset (Fig. 2a) is generally well-represented by the FINE-FOR (Fig. 2b) simulation. The model captures such features as the rainfall maxima along coastal British Columbia, Washington, northwest California, and the Sierra Nevada. However, in Oregon, the simulated rainfall maximum is about 100 km inland from the maximum in the PGF data. Precipitation is generally overestimated in the rain shadow on the eastern side of the Rockies and underestimated along the east coast of North America. The FINEV-FOR simulation is very similar to FINE-FOR in the western US, but gives slightly improved precipitation estimates in the Midwest (Fig. 2c). The XFINE-FOR simulation (Fig. 2d) is a better match to the PGF data than FINE-FOR in that (1) it yields larger precipitation amounts for the Appalachian Mountain region, and

(2) the rainfall maximum in Oregon shifts closer to the coast. The COARSE-FOR simulation generally gives lower rainfall values than the other simulations, leading to underprediction of the rainfall maximum on the west coast and exacerbating the underprediction on the east coast (Fig. 2e). However, it gives a better simulation of the low precipitation values in the rain shadow of the Rockies.

The PGF temperature dataset (Fig. 3a) was well-simulated by FINE-FOR (Fig. 3b) for most of the US. However, one notable bias occurred for parts of the Great Basin, where the model was too cool. This is potentially related to biases in the 1º SST data, especially near relatively small-scale features like the Gulf of California (Kim et al., in prep.). Most of the nearby offshore temperatures were also lower in the simulations than in the PGF, and advection of this relatively cool air may be biasing the model over land. A second bias was that the model was too warm in eastern Canada. Temperature biases in FINEV-FOR (Fig. 3c), XFINE-FOR (Fig. 3d) and COARSE-FOR (Fig. 3e) were similar to those in FINE-FOR.

The Pacific Northwest relies heavily on winter snowfall to provide water for the summer months because there is relatively little summer precipitation. To measure snow water equivalent (SWE), the US Department of Agriculture's Natural Resources Conservation Service maintains a network of snow courses throughout Oregon, Washington, Idaho, and other western states. The earliest records go back to 1915. The California Department of Water Resources has an independent network of snow courses. Details on the measurements have been previously published (Clark et al. 2001; McCabe and Dettinger 2002). Mote (2003) reported that SWE on April 1st has typically ranged from 40-50 cm for the past ~25 years for a region that include mountainous areas of

Oregon, Washington, and Idaho. In California, Howat and Tulaczyk (2005) found peak SWE of about 120 cm along much of the central spine of the Sierra Nevada.

We compared these observation-based numbers to values simulated by OLAM, considering the higher-resolution simulations first. The corresponding April 1st SWE simulated in XFINE-FOR averaged over 1999-2012 is shown in Fig. 4a. Values in the Northwest are generally consistent with the observed values, and ranged from about 65 cm in the southern Cascades, to about 20 cm in northwest Oregon, to about 50 cm in western Idaho. Peak values along the Sierra Nevada reached 100-120 cm and are also consistent with observations. The simulation with enhanced vertical resolution, FINEV-FOR, also gave reasonable results for central California (Fig. 4b), but gave less SWE than XFINE-FOR in other sectors. In contrast, simulated values from FINE-FOR were much lower (Fig. 4c), which is unsurprising given its coarser representation of topography (Leung and Qian 2003). Peak SWE in southern Oregon and the Sierra Nevada reached only 50 cm. Finally, in COARSE-FOR, simulated SWE was less than 35 cm throughout the western US, and was negligible in California (Fig. 4d). These results show that the quality of the simulation of snowpack degrades sharply with coarsening model resolution. For this reason, we limit the remainder of our analysis of snowpack to the XFINE and FINEV pairs of simulations.

b. Impacts of deforestation on surface climate

We found that FINE-DEF had a large, statistically significant precipitation deficit relative to FINE-FOR throughout the Pacific Northwest (Fig. 5a). Precipitation differences were typically 10-20% (or 1-2 mm day^{-1}) and reached up to 30%. There was also a comparable precipitation deficit along the western slopes of the Sierra Nevada range, but this difference was not statistically significant at the 95% confidence level. In the finest-resolution simulations, XFINE-DEF had large precipitation deficits relative to XFINE-FOR, and these precipitation deficits were indeed statistically significant near the Sierra Nevada as well as in the Pacific Northwest (Fig. 5b). Differences between FINEV-DEF and FINEV-FOR (not shown) were very similar to the differences between FINE-DEF and FINE-FOR. Finally, in the combined ensemble consisting of FINE, FINEV, and XFINE, the region with statistically significant precipitation deficits encompasses Washington, Oregon, Idaho, northern California, and Nevada (Fig. 5c). Our analysis of the COARSE pair of simulations led to very different results (Fig. 5d). In this case, the COARSE-DEF actually had more precipitation than COARSE-FOR in the Northwest US, although this difference was not statistically significant. The effects of model resolution will be discussed in more detail below.

We also computed changes in other important hydroclimatic variables, including evapotranspiration, moisture convergence, and temperature. The precipitation deficits in the western US occurred almost entirely because of changes in moisture convergence in the FINE simulation pair (Fig. 6a), while changes in evapotranspiration were much smaller for all grid cells (Fig. 6b). Similar results held for the FINEV, and XFINE simulation pairs (not shown). In the Northwest US, FINE-DEF was generally about 0.5°C cooler than FINE-FOR (Fig. 6c). However, these changes were generally not statistically significant in the locations where the largest precipitation changes occurred, including western Washington, western Oregon, and California. Temperature differences between XFINE-DEF and XFINE-FOR were small, generally of magnitude less than 0.2°C in the western US (Fig. 6d). These temperature differences were only statistically significant in the southeast US. Temperature differences between FINEV-DEF and FINEV-FOR and between COARSE-DEF and COARSE-FOR were also small and generally not statistically significant (not shown).

Given the large decreases in precipitation and relatively small changes in temperature in the XFINE simulation pair, we expected that SWE would decrease in the mountains of the Northwest US and the Sierra Nevada. The April 1st SWE averaged over 1999-2012 from XFINE-FOR and XFINE-DEF are shown in Figs. 4a and 4f, respectively. SWE from XFINE-DEF is much lower than in XFINE-FOR. Values over the central Sierra Nevada are reduced by about half, with values in XFINE-DEF generally ranging from 30-90 cm. In XFINE-DEF, snowpack no longer exists in parts of northern California and is reduced by over 50% in southern Oregon, but areas farther north and east were not strongly affected. Similar results were obtained for the FINEV simulation pair, with FINEV-FOR (Fig. 4b) having much more snowpack than FINE-DEF (Fig. 4f).

c. Comparison to El Niño

The simulated reductions in precipitation in the Northwest US resulted from Amazon deforestation, but similar precipitation anomalies are commonly observed during El Niño events (Redmond and Koch 1991). We now pursue this analogy a bit further. During the DJF, precipitation in the Northwest is strongly controlled by the jet stream position. However, in El Niño years, the jet has an increased tendency to split into two branches, with one over the Queen Charlotte Islands and the other over the southern tier of the US, bringing wetter conditions to British Columbia and to the Southwest US. In the FINE simulations, deforestation resulted in positive anomalies of 1-3 m s^{-1} in the 250 hPa zonal winds for northern British Columbia and northern Mexico, while negative anomalies of 2-4 m s^{-1} were evident over the Pacific Northwest (Fig. 7a). These changes were statistically significant, but hatching was omitted from the figure to reduce visual clutter. Thus, as with El Niño, deforestation modifies the jet stream so as to divert storms either to the north or south of the Northwest US. This is consistent with the simulated precipitation reductions in the Northwest US (Fig. 5a). In the XFINE simulation pair, deforestation also causes a reduction in 250 hPa zonal wind speed over the western US (Fig. 7b). However, the magnitudes of the changes are about 1 m s^{-1} smaller and are shifted to the south relative to the FINE simulation pair. The FINEV simulation pair was very similar to the FINE simulation pair, and for simplicity we will not consider it further.

The Southeast US is also typically affected by El Niño, and experiences relatively cool, wet conditions during DJF (Ropelewski and Halpert 1987, 1989). These conditions arise because of a stronger, more southerly jet stream. In the FINE simulations (Fig. 7a), we see that deforestation caused the southern flank of the jet over the southeastern US to be strengthened by 2-4 m s^{-1}. In the XFINE simulations (Fig. 7b), the southern flank of the jet over the southeastern US strengthens by 1-2 m s^{-1}, while the jet weakens by a similar amount over Quebec. As with El Niño, this change brings cooler temperatures to the southeastern US. However, unlike during El Niño, the southeast is simulated to be drier in the deforested simulation than in the forested simulation. This situation arises because of the influx of cool, dry air from the north.

d. Planetary scale impacts

Although our focus has been on North America, where our grid mesh has fine resolution, we found that the changes in the jet stream described above are part of a planetary-scale set of changes generated by Amazon deforestation. We illustrate our results with the FINE simulation pair; the XFINE pair is similar except where noted. As reported in many previous studies, we find that deforestation acts to increase near-surface temperatures in the deforested region (Fig. 8a). This heating leads to increases in the 850-300 hPa thickness (Fig. 8b), and extends nearly tropics-wide (Held and Hou 1980). Previous idealized experiments have demonstrated how a tropical heating anomaly can act as a source of Rossby waves that can propagate from the tropics to the extratropics (Hoskins and Karoly 1981; Jin and Hoskins 1995; Held et al. 2002). Indeed, examination of the deforestation-induced changes in the 250 hPa (Fig. 9a) and 850 hPa (Fig. 9b) wind fields reveals that wave trains were excited in both hemispheres, with the higher-amplitude wave train in the northern (winter) hemisphere. These changes bear marked similarities to the idealized experiments of Jin and Hoskins (1995), who carried out numerous simulations investigating the impacts of tropical tropospheric heating anomalies. When they placed a heating source over the Amazon, they found that Rossby wave trains were excited that propagated into both hemispheres, and that North America in particular was affected.

Jin and Hoskins (1995) also found that there was an upper-level negative vorticity anomaly in the northern vicinity of their heating source and a positive vorticity anomaly in the southern vicinity of their heating source. The reverse configuration was realized at low levels. We obtained very similar results here. Our southern upper-level anomaly is located south of the deforested region and spans approximately from 90°-40°W (Fig. 9a).

Our northern upper-level anomaly is located in the northern part of the deforested area and is more limited in spatial extent, perhaps due to constraints imposed by the Andes (Fig. 9a). Our lower-level northern anomaly is evident in the northern part of the deforested region, though our lower-level southern anomaly, just south of the deforested area, is weak (Fig. 9b). Results from the XFINE simulation pair (Figs. 9c-d) are broadly similar, with the main differences being slightly stronger lower-level anomalies and slightly weaker upper-level anomalies in the deforested sector.

In the COARSE simulation pair, deforestation also generates wave trains (Fig. 10), but these are nearly 180° out of phase with the FINE and XFINE wave trains throughout the midlatitudes. To quantify this, we interpolated the 250 hPa meridional wind fields from FINE, XFINE, and COARSE onto a common 3° longitude by 3° latitude grid, and then computed the Spearman's ρ correlation coefficients between FINE and XFINE and between FINE and COARSE for all grid cells between 30°-48°N. We found a positive correlation ($\rho=0.27$; $p < 1\text{x}10^{-5}$) between FINE and XFINE and a negative correlation ($\rho=-0.28$; $p < 1\text{x}10^{-5}$) between FINE and COARSE. Unsurprisingly then, the COARSE simulation pair gave a (not statistically significant) increase in precipitation for northwestern North America, rather than an increase (Fig. 5d). These differences between COARSE and FINE are consistent with previous work that underlined the importance of a high-resolution representation of topography for the simulation of Amazon precipitation (Medvigy et al. 2008) and local impacts of deforestation (Ramos da Silva et al. 2008; Medvigy et al. 2011).

4. Discussion and conclusions

This work has focused on some potential extratropical responses to the complete deforestation of the Amazon. We find that precipitation in the Northwest US and in parts of California is strongly reduced during DJF because of deforestation. Such an effect has not been seen in previous analyses (Gedney and Valdes 2000; Werth and Avissar 2002; Avissar and Werth 2005; Findell et al. 2006; Hasler et al. 2009). A critical difference between our simulations and previous simulations is the model resolution. Whereas previous work was carried out at resolutions of about 200 km, we studied simulations that used a mesh with a characteristic length scale of 25-50 km for much of North and South America. This permits the simulation of regional scale circulations in the Amazon that are important for the propagation of waves from the tropics to the extratropics. When we ran simulations at a resolution typical of previous studies, the wave trains resulting from deforestation had a different phase and their extratropical impacts were strongly reduced.

In this study, we confirm a suggestion made by Avissar and Werth (2005) that substantial similarities may exist between the extratropical effects of Amazon deforestation and of El Niño. Like El Niño, we find that Amazon deforestation has a widespread warming effect on the tropical troposphere (Seager et al. 2003), and this generates Rossby wave trains in both hemispheres. The implication of this for western North America is that storms tend to be diverted to the north and south of the path that they would have followed in the absence of deforestation. Western Washington and Oregon receive much less precipitation. However, the extratropical signature of deforestation extends farther south than that of El Niño, and consequently the Sierra Nevada are also strongly impacted by deforestation. Furthermore, because temperatures do not drastically change, snowpack on the Sierra Nevada is markedly reduced. These changes are co-located with significant topography, and the historical precipitation record can only be reproduced in OLAM if this topography is represented at fine enough resolution.

To the extent that our simulations are consistent with reality, the deforestation of the Amazon will have enormous consequences for the irrigation-fed agriculture in California. In the US, agriculture and food sectors contribute 4.8% of the gross domestic product and are the source of 15.8 million jobs nationwide. California has been the nation’s number one state for food and dairy production during the past 50 years. The ability of California to maintain its large output is directly related to the availability of irrigation water (Draper et al. 2003). Our work complements the many previous studies that have investigated the impact of climate warming on California hydrology (Lettenmaier and Gan 1990; Kim et al. 2002; Maurer 2007). In response to increases in greenhouse gases, climate models have consistently simulated a warmer, slightly wetter California, with overall reduced end-of-winter snowpack. Our simulations indicate that Amazon deforestation would likely exacerbate this snowpack reduction.

Natural ecosystems would also be strongly affected by the rainfall reductions simulated here. In the relatively wet forests of western Oregon and Washington, fires are relatively rare. However, fuel accumulations are high, and when fires do occur, they can lead to complete stand replacement (Mote et al. 2003). In California, the California Floristic Province has been designated as one of 33 global biodiversity hotspots as a result of its large number of native and endemic species (Myers et al. 2000). Drawdown of freshwater resources is one of the principal threats facing the area.

This study represents an initial effort at using a high-resolution GCM to investigate inter-continental effects of Amazon deforestation, and raises many important questions. First, our experiment design was simplified in that it considered the complete deforestation of the Amazon. However, about 40% of the Brazilian Amazon is in some form of a protected area (Walker et al. 2009), and deforestation may be less severe in these areas. Furthermore, actual future spatial patterns of deforestation may be complex (Soares-Filho et al. 2006) and induce local or even regional scale circulations. Thus, future analyses should consider more realistic spatial patterns of deforestation. Second, our simulations used relatively coarse resolution over most of the world outside of the Americas. Pursuing the analogy of Amazon deforestation with El Niño, additional Amazon deforestation experiments should be carried out using model grid meshes with fine resolution over areas known to be sensitive to El Niño. Third, our model simulations were designed to isolate the impacts of Amazon deforestation and so they did not consider the effects of changes in greenhouse gases. Assessing the combined effect of Amazon deforestation and greenhouse gas increases on the Northwest US and California should be a priority. Fourth, there are a number of physical processes that were either parameterized, like cumulus convection, or not represented at all, like fires, aerosol effects, and the dynamic responses of terrestrial ecosystems. These are all processes that merit future attention. Fifth, our simulations were driven by historical SSTs and so they did not account for ocean feedbacks. Coupled atmosphere-ocean GCMs should be used to assess the extent to which the ocean can buffer (or exacerbate) the changes simulated here. Sixth, though our precipitation changes were statistically significant, additional runs, especially those carried out with independent models, would bolster this assessment.

Acknowledgments

The authors gratefully acknowledge support from National Science Foundation Awards 1151102 (to D.M.) and 0902197 (to R.A. and R.L.W.). NCEP Reanalysis 2 data were provided by the NOAA/OAR/ESRL PSD, Boulder, Colorado, USA, from their Web site at http://www.esrl.noaa.gov/psd/. The simulations presented in this article were performed on computational resources supported by the PICSciE-OIT High Performance Computing Center and Visualization Laboratory at Princeton University.

References

Andreae, M.O., D. Rosenfeld, P. Artaxo, A.A. Costa, G.P. Frank, K.M. Longo, and M.A.F. Silva-Dias, 2004: Smoking rain clouds over the Amazon. *Science*, **303**, 1337-1342.

Avissar, R., and D. Werth, 2005: Global hydroclimatological teleconnections resulting from tropical deforestation. *J. Hydrometeorol.*, **6**, 134-145.

Cayan, D.R., 1996: Interannual climate variability and snowpack in the western United States. *J. Climate*, **9**, 928-948.

Clark, M.P., M.C. Serreze, and G.J. McCabe, 2001: Historical effects of El Nino and La Nina events on the seasonal evolution of the montane snowpack in the Columbia and Colorado River Basins. *Water Resour. Res*., **37**, 741-757.

Costa, M.H., and J.A. Foley, 2000: Combined effects of deforestation and doubled atmospheric CO2 concentrations on the climate of Amazonia. *J. Climate*, **13**, 18-34.

Dai, A., K.E. Trenberth, and T.R. Karl, 1998: Global variations in droughts and wet spells: 1900-1995. *Geophys. Res. Lett*., **25** (17), 3367-3370.

Draper, A.J., M.W. Jenkins, K.W. Kirby, J.R. Lund, and R.E. Howitt, 2003: Economic-engineering optimization for California water management. *J. Water Resour. Plan. Manage*., **129**, 155-164.

Enfield, D.B., A.M. Mestas-Nuñez, and P.J. Trimble, 2001: The Atlantic multidecadal oscillation and its relation to rainfall and river flows in the continental U.S. *Geophys. Res. Lett*., **28** (10), 2077-2080.

Findell, K.L., T.R. Knutson, and P.C.D. Milly, 2006: Weak simulated extratropical responses to complete tropical deforestation. *J. Climate*, **19**, 2835-2850.

Gandu, A.W., J.C.P. Cohen, and J.R.S. Souza, 2004: Simulation of deforestation in eastern Amazonia using a high-resolution model. *Theor. Appl. Climatol*., **78**, 123-135.

Gash, J.H.C., and C.A. Nobre, 1997: Climatic effects of Amazonian deforestation: some results from ABRACOS. *Bull. Amer. Meteor. Soc*., **78**, 823-830.

Gedney, N., and P.J. Valdes, 2000: The effect of Amazonian deforestation on the northern hemisphere circulation and climate. *Geophys. Res. Lett.*, **27**, 3053-3056.

Hahmann, A.N., and R.E. Dickinson, 1997: RCCM2-BATS model over tropical South America: Applications to tropical deforestation. *J. Climate*, **10**, 1944-1964.

Harrison, D.E., and N.K. Larkin, 1998: Seasonal U.S. temperature and precipitation anomalies associated with El Nino: Historical results and comparison with 1997-98. *Geophys. Res. Lett*., **25** (21), 3959-3962.

Hasler, N., D. Werth, and R. Avissar, 2009: Effects of tropical deforestation on global hydroclimate: a multimodel ensemble analysis. *J. Climate*, **22**, 1124-1141.

Held, I., and A.Y. Hou, 1980: Nonlinear axially symmetric circulations in a nearly inviscid atmosphere. *J. Atmos. Sci*., **37**, 515-533.

Held, I.M., M. Ting, and H. Wang, 2002: Northern winter stationary waves: theory and modeling. *J. Climate*, **15**, 2125-2144.

Henderson-Sellers, A., R.E. Dickinson, T.B. Durbidge, P.J. Kennedy, K. McGuffie, and A.J. Pitman, 1993: Tropical deforestation – modeling local-scale to regional-scale climate change. *J. Geophys. Res.*, **98**, 7289-7315.

Hoerling, M.P., and M. Ting, 1994: Organization of extratropical transients during El Niño. *J. Climate*, **7**, 745-766.

Hollander, M., and D.A. Wolfe, 1999: *Nonparametric Statistical Methods*. John Wiley and Sons, 787 pp.

Hoskins, B.J., and D.J. Karoly, 1981: The steady linear response of a spherical atmosphere to thermal and orographic forcing. *J. Atmos. Sci*., **38**, 1179-1196.

Howat, I.M., and S. Tulaczyk, 2005: Climate sensitivity of spring snowpack in the Sierra Nevada. *J. Geophys. Res*., **110**, F04021, doi:10.1029/2005JF000356.

Jin, F., and B.J. Hoskins, 1995: The direct response to tropical heating in a baroclinic atmosphere. *J. Atmos. Sci*., **52**, 307-319.

Kain, J.S., 2004: The Kain-Fritsch convective parameterization. *J. Appl. Meteorol*., **43**, 170-181.

Kalnay, E., and Coauthors, 1996: The NCEP/NCAR 40-year reanalysis project. *Bull. Am. Meteorol. Soc*., **77**, 437-470.

Kim, J., T.K. Kim, R.W. Arritt, and N.L. Miller, 2002: Impacts of increased CO_2 on the hydroclimate of the western United States. *J. Climate*, **15**, 1926-1943.

Kim, S.H. D.H. Stack, J. Kim, A.K. Prasad, H.M. El-Askary, N. Hatzopoulos, D. Medvigy, C. Tremback, R.L. Walko, G. Asrar, and M. Kafatos. Impact of the Gulf of California SST on simulating precipitation and crop productivity in the Southwestern United States. To be submitted to *J. Geophys. Res*., Fall 2012.

Lean, J., and P.R. Rowntree, 1993: A GCM simulation of the impact of Amazonian deforestation on climate using an improved canopy representation. *Quart. J. Roy. Meteor. Soc*., **119**, 509-530.

Lettenmaier, D.P., and T.Y. Gan, 1990: Hydrologic sensitivities of the Sacramento-San Joaquin River basin, California, to global warming. *Water Resour. Res*., **26**, 69-86.

Leung, L.R., and Y. Qian, 2003: The sensitivity of precipitation and snowpack simulations to model resolution via nesting in regions of complex terrain. *J. Hydrometeorol*., **4**, 1025-1043.

Leung, L.R., Qian, Y., and X. Bian, 2003a: Hydroclimate of the western United States based on observations and regional climate simulation of 1981-2000. Part I: Seasonal statistics. *J. Climate*, **16**, 1892-1911.

Leung, L.R., Qian, Y., Bian, X., and A. Hunt, 2003b: Hydroclimate of the western United States based on observations and regional climate simulation of 1981-2000. Part II: Mesoscale ENSO anomalies. *J. Climate*, **16**, 1912-1928.

Ljung, G.M., and G.E.P. Box, 1978: On a measure of lack of fit in time series models. *Biometrika*, **65**, 297-303.

Lu, J., G. Chen, and D.M.W. Frierson, 2008: Response of the zonal mean atmospheric circulation to El Niño versus global warming. *J. Climate*, **21**, 5835-5851.

Maurer, E.P., 2007: Uncertainty in hydrologic impacts of climate change in the Sierra Nevada, California, under two emissions scenarios. *Climatic Change*, **82**, 309-325.

McCabe, G.J., and M.D. Dettinger, 2002: Primary models and predictability of year-to-year snowpack variations in the western United States from teleconnections with Pacific Ocean climate. *J. Hydrometeorol*., **3**, 13-25.

McCabe, G.J., M.A. Palecki, and J.L. Betancourt, 2004: Pacific and Atlantic Ocean influences on the multidecadal drought frequency in the United States. *Proc. Natl. Acad. Sci. USA*, **101**, 4136-4141.

Medvigy, D., R.L. Walko, and R. Avissar, 2008: Modeling interannual variability of the Amazon hydroclimate. *Geophys. Res. Lett*., **35**, L15817, doi:10.1029/2008GL034941.

Medvigy, D., R.W. Walko, M.J. Otte, and R. Avissar, 2010: The Ocean-Land-Atmosphere Model (OLAM): optimization and evaluation of simulated radiative fluxes and precipitation. *Mon. Weather Rev.*, **138**, 1923-1939.

Medvigy, D., R.L. Walko, and R. Avissar, 2011: Effects of deforestation on spatiotemporal distributions of precipitation in South America. *J. Climate*, **24**, 2147-2163.

Medvigy, D., R.L. Walko, and R. Avissar, 2012: Simulated links between deforestation and extreme cold events in South America. *J. Climate*, **25**, 3851-3866.

Mote, P.W., and Coauthors, 2003: Preparing for climatic change: the water, salmon, and forests of the Pacific Northwest. *Climatic Change*, **61**, 45-88.

Myers, N., R.A. Mittermeier, C.G. Mittermeyer, G.A.B. da Fonseca, and J. Kent, 2000: Biodiversity hotspots for conservation priorities. *Nature*, **403**, 853-858.

Olson, J.S., 1994a: Global ecosystem framework-definitions: USGS EROS Data Center Internal Report, Sioux Falls, SD, 37 p.

Olson, J.S., 1994b: Global ecosystem framework-translation strategy: USGS EROS Data Center Internal Report, Sioux Falls, SD, 39 p.

R Development Core Team, 2008: R: A language and environment for statistical computing. R Foundation for Statistical Computing, Vienna, Austria. ISBN 3-900051-07-0, URL http://www.R-project.org.

Ramos da Silva, R., D. Werth, and R. Avissar, 2008: Regional impacts of future land-cover changes on the Amazon basin wet-season climate. *J. Climate*, **21**, 1153-1170.

Randall, D.A., and Coauthors, 2007: Climate models and their evaluation. In: *Climate Change 2007: The Physical Science Basis. Contribution of Working Group I to the Fourth Assessment Report of the Intergovernmental Panel on Climate Change* [Solomon, S., D. Qin, M. Manning, Z. Chen, M. Marquis, K.B. Averyt, M. Tignor, and H. L. Miller (eds.)]. Cambridge University Press, Cambridge, United Kingdom, New York, NY, USA.

Redmond, K.T., and R.W. Koch, 1991: Surface climate and streamflow variability in the western United States and their relationship to large-scale circulation indices. *Water Resour. Res.*, **27**, 2381-2399.

Reynolds, R.W., N.A. Rayner, T.M. Smith, T.C. Stokes, and W. Wang, 2002: An improved in situ and satellite SST analysis for climate. *J. Climate*, **15**, 1609-1625.

Ropelewski, C.F., and M.S. Halpert, 1987: Global and regional scale precipitation patterns associated with the El Niño/Southern Oscillation. *Mon. Wea. Rev.*, **115**, 1606-1626.

Ropelewski, C.F., and M.S. Halpert, 1989: Precipitation patterns associated with the high index phase of the Southern Oscillation. *J. Climate,* **2**, 268-284.

Royston, P, 1982: An extension of Shapiro and Wilk's W test for normality to large samples. *Appl. Statist.*, **31**, 115-124.

Sampaio, G., C. Nobre, M.H. Costa, P. Satyamurty, B.S. Soares-Filho, and M. Cardoso, 2007: Regional climate change over eastern Amazonia caused by pasture and soybean cropland expansion. *Geophys. Res. Lett.*, **34**, L17709, doi:10.1029/2007GL030612.

Seager, R., N. Harnik, Y. Kushnir, W. Robinson, and J. Miller, 2003: Mechanisms of hemispherically symmetric climate variability. *J. Climate*, **16**, 2960-2978.

Seager, R., N. Narnik, W.A. Robinson, Y. Kushnir, M. Ting, H.-P. Huang, and J. Velez, 2005: Mechanisms of ENSO-forcing of hemispherically symmetric precipitation variability. *Q. J. R. Meteorol. Soc*., **131**, 1501-1527.

Seager, R., Y. Kushnir, J. Nakamura, M. Ting, and N. Naik, 2010: Northern hemisphere winter snow anomalies: ENSO, NAO and the winter of 2009/10. *Geophys. Res. Lett.*, **37**, L14703, doi:10.1029/2010GL043830.

Sheffield, J., G. Goteti, and E.F. Wood, 2006: Development of a 50-year high-resolution global dataset of meteorological forcings for land surface modeling. *J. Climate*, **19**, 3088-3111.

Soares-Filho, B.S., and Coauthors, 2006: Modelling conservation in the Amazon basin. *Nature*, **440**, 520-523.

Walker, R., N.J. Moore, E. Arima, S. Perz, C. Simmons, M. Caldas, D. Vergara, and C. Bohrer, 2009: Protecting the Amazon with protected areas. *Proc. Natl. Acad. Sci. USA*, **106**, 10582-10586.

Walko, R. L., and R. Avissar, 2008a: The Ocean-Land-Atmosphere Model (OLAM): Shallow Water Tests. *Mon. Wea. Rev.*, **136**, 4033-4044.

Walko, R. L., and R. Avissar, 2008b: The Ocean-Land-Atmosphere Model (OLAM): Formulation and Tests of the Nonhydrostatic Dynamic Core. *Mon. Wea. Rev.*, **136**, 4045-4062.

Walko, R.L, and R. Avissar, 2011: A direct method for constructing refined regions in unstructured conforming triangular-hexagonal computational grids: application to OLAM. *Mon. Wea. Rev*., **139**, 3923-3937.

Wallace, J.M., Smith, C., and C.S. Bretherton, 1992: Singular value decomposition of wintertime sea surface temperature and 500-mb height anomalies. *J. Climate*, **14**, 2659-2674.

Werth, D., and R. Avissar, 2002: The local and global effects of Amazon deforestation. *J. Geophys. Res.*, **107**, 8087, doi:/10.1029/2001JD000717.

Williams, E., and Coauthors, 2002: Contrasting convective regimes over the Amazon: Implications for cloud electrification. *J. Geophys. Res*., **107**, 8082, doi:10.1029/2001JD000380.

Zhang, Y., Qian, Y., Dulière, V., Salathé Jr, E.P., and L.R. Leung, 2012: ENSO anomalies over the western United States: present and future patterns in regional climate simulations. *Climatic Change*, **110**: 315-346.

Tables

Table 1: Description of the numerical simulations used in this study. “CLS” is the characteristic length scale of the grid mesh.

Simulation	CLS (Andes and Amazon)	CLS (United States)	Maximum vertical resolution	Amazon land cover
FINE-FOR	50 km	50 km	200 m	From the 1990s
FINE-DEF	50 km	50 km	200 m	Complete deforestation
FINEV-FOR	50 km	50 km	100 m	From the 1990s
FINEV-DEF	50 km	50 km	100 m	Complete deforestation
XFINE-FOR	50 km	25 km	200 m	From the 1990s
XFINE-DEF	50 km	25 km	200 m	Complete deforestation
COARSE-FOR	200 km	200 km	200 m	From the 1990s
COARSE-DEF	200 km	200 km	200 m	Complete deforestation

Figure Captions

(For now, I've only included captions below the figures. When it is time for submission, I will copy and paste the final versions of the captions here.)

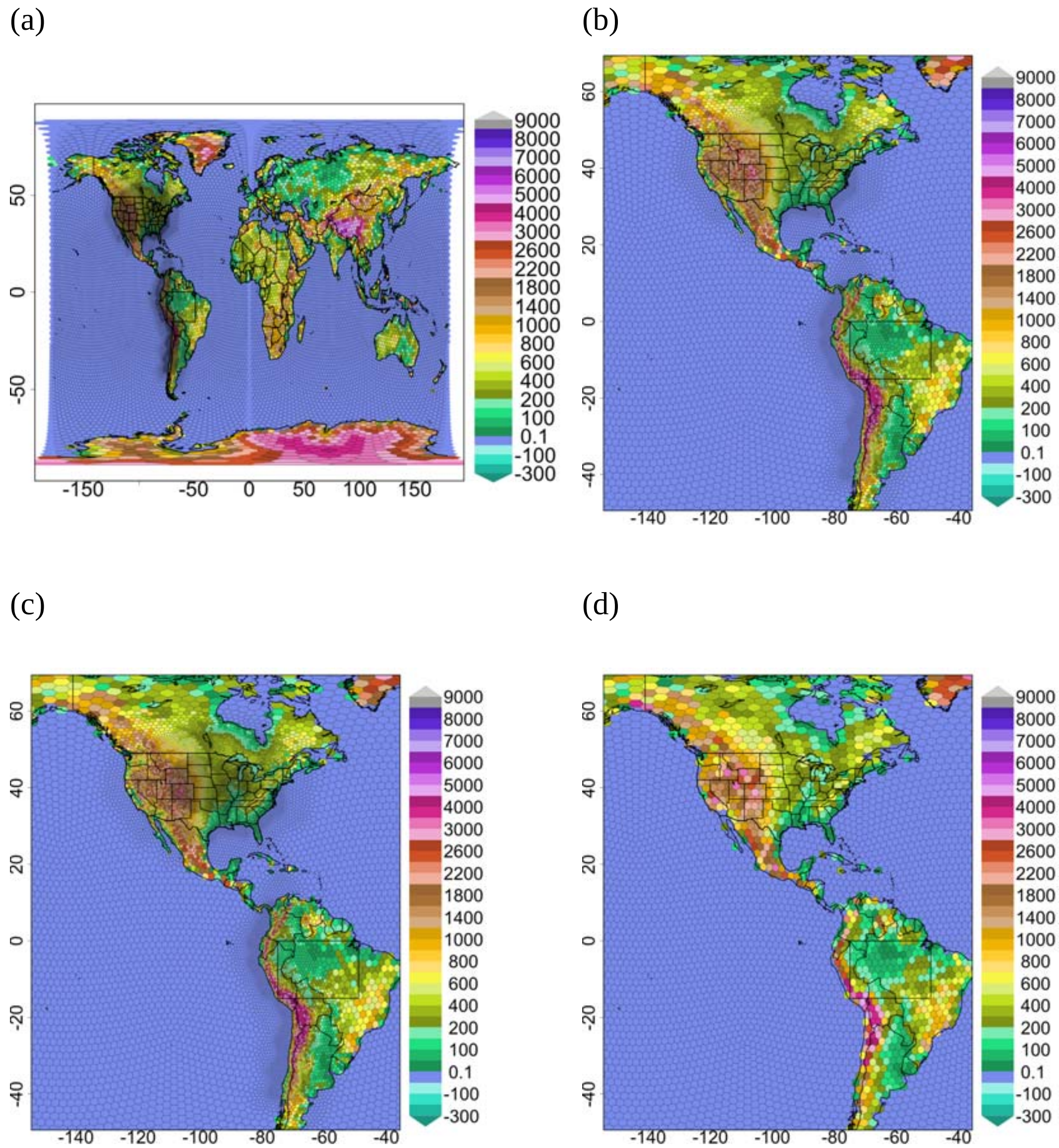

FIGURE 1: OLAM grid mesh and topography (m) for the different simulations. Panel a: FINE pair, global. Panel b: FINE pair, Americas. Panel c: XFINE pair, Americas. Panel d: COARSE pair, Americas. Away from the Americas, the XFINE and COARSE meshes are very similar to panel a. The boxes over South America denote the deforested region.

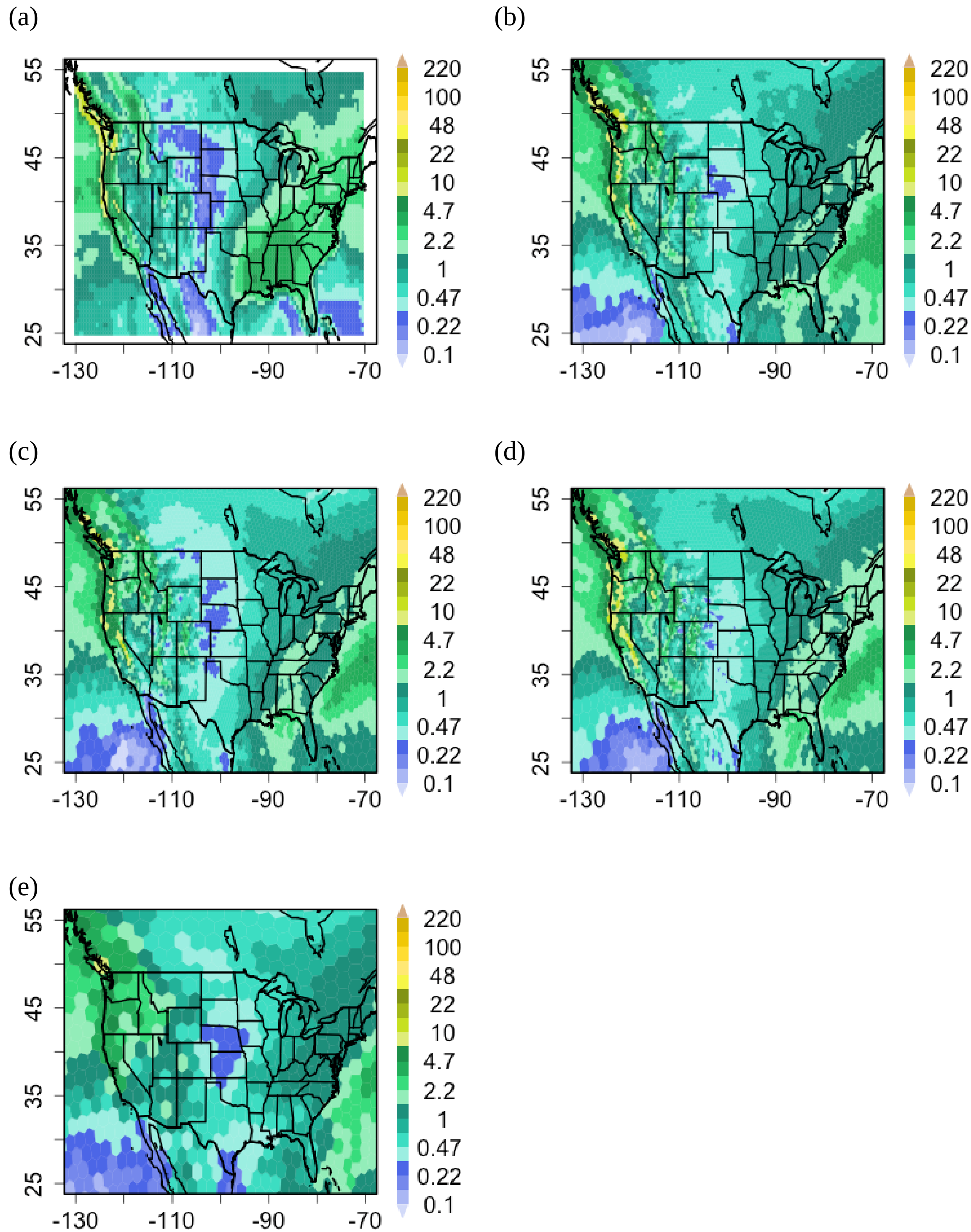

FIGURE 2: December-January-February mean daily precipitation (mm day^{-1}) as represented in the Princeton Global Forcings (PGF) dataset (panel a) and as simulated by

the OLAM model. Panel b: results from FINE-FOR, which has 50 km characteristic length scale (CLS) over the US. Panel c: results from FINEV-FOR, which has enhanced vertical resolution. Panel d: results from XFINE-FOR, which has enhanced horizontal CLS. Panel e: results from COARSE-FOR, which has coarse horizontal CLS.

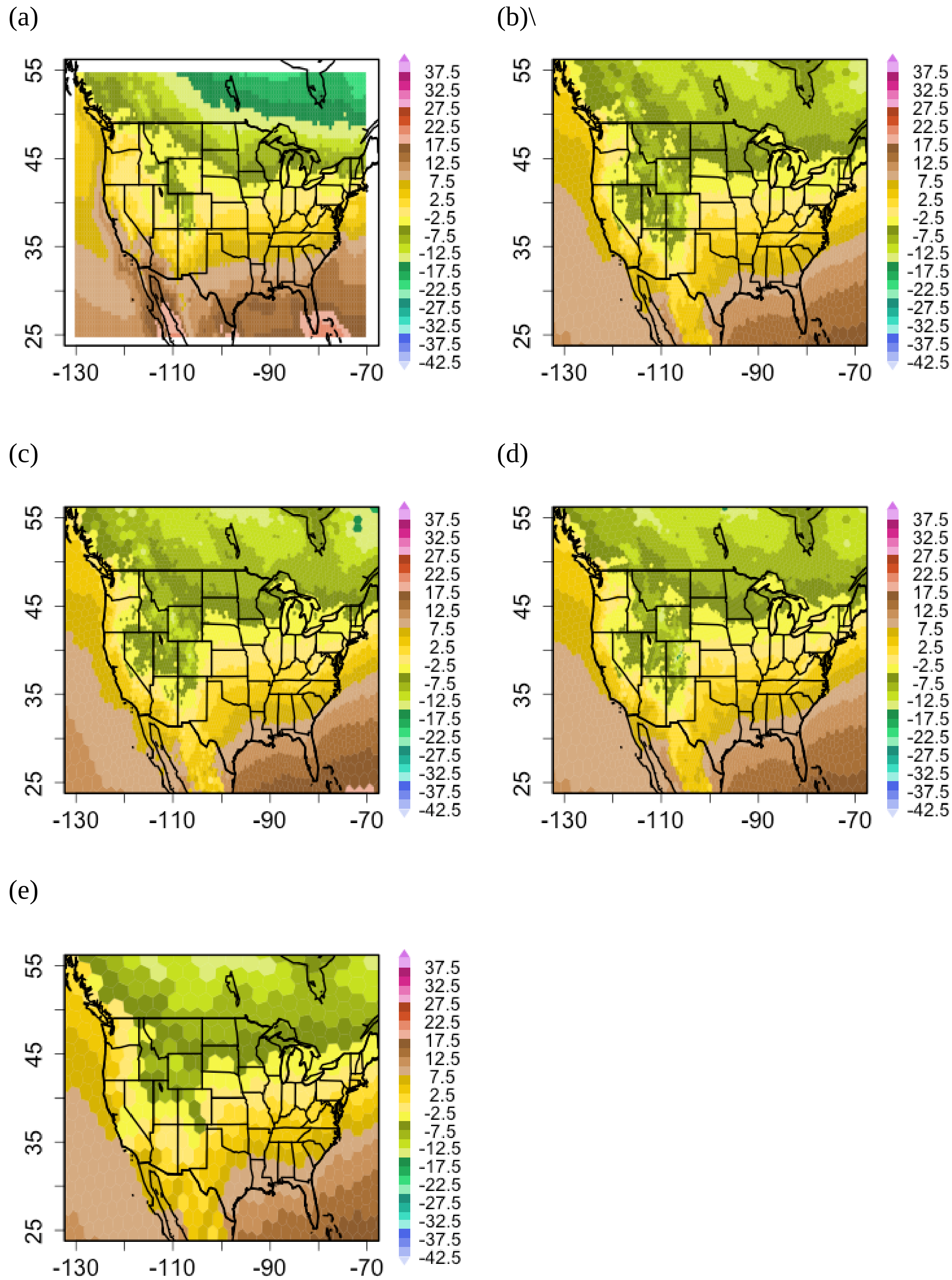

FIGURE 3: Like Figure 2, but for daily mean near-surface temperature (°C).

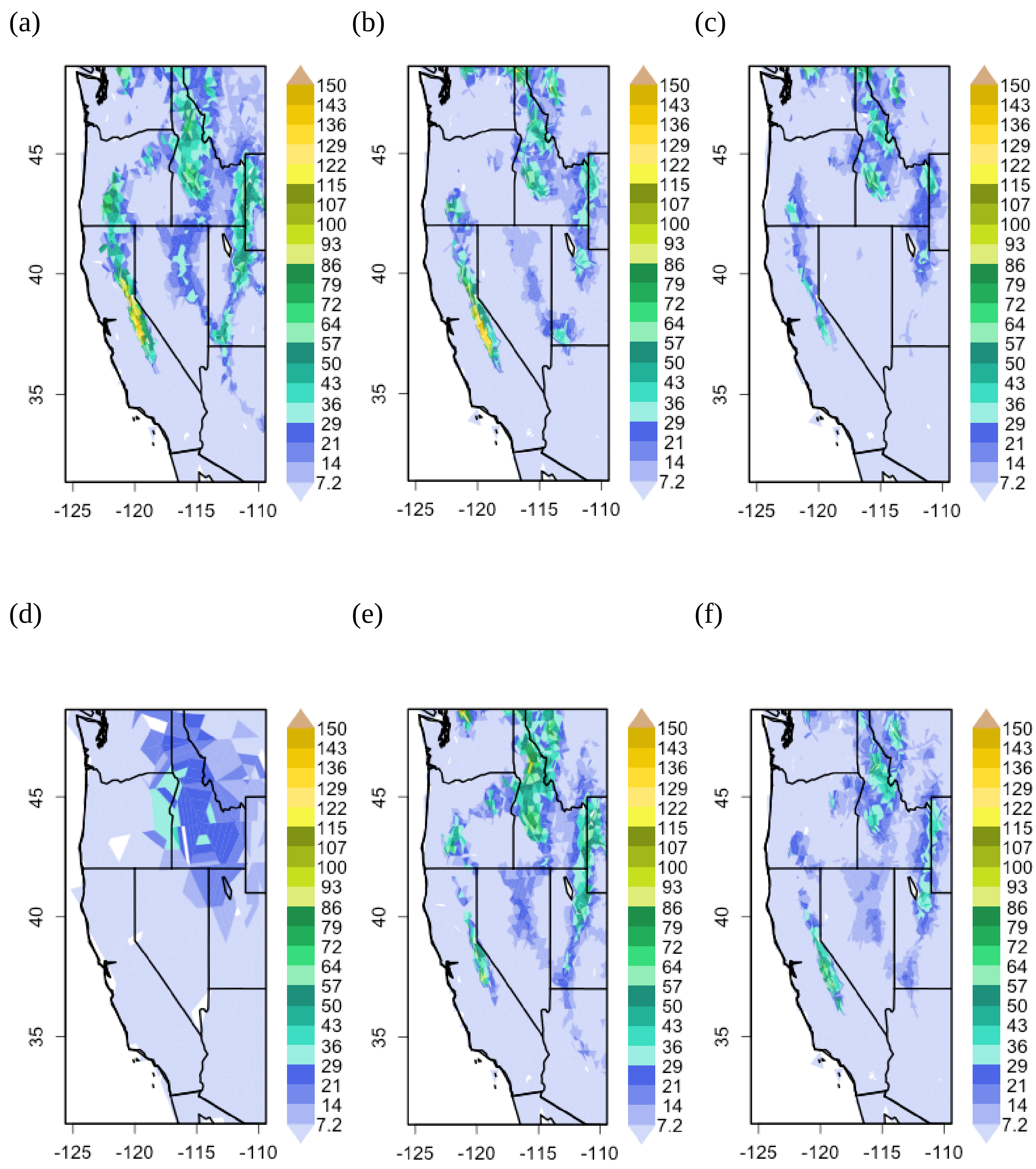

FIGURE 4: Average April 1st snow water equivalent (cm) as simulated in the XFINE-FOR (panel a), FINEV-FOR (panel b), FINE-FOR (panel c), COARSE-FOR (panel d), XFINE-DEF (panel e), and FINEV-DEF (panel f) simulations.

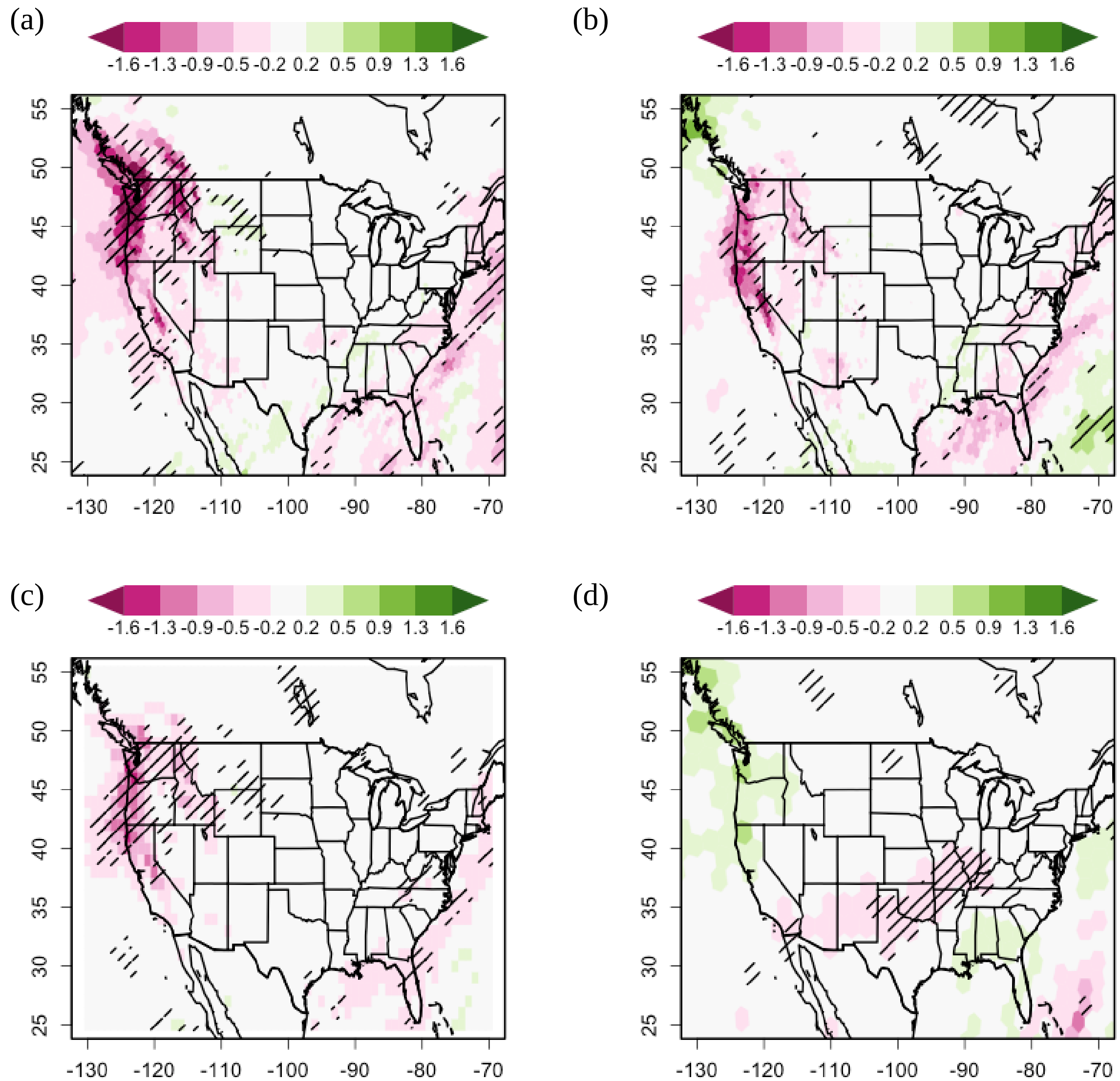

FIGURE 5: Simulated changes in daily mean precipitation (mm day^{-1}) from the FINE (panel a), XFINE (panel b), combined FINE, FINEV, and XFINE (panel c), and COARSE (panel d) simulation pairs. Areas with statistically significant changes are hatched.

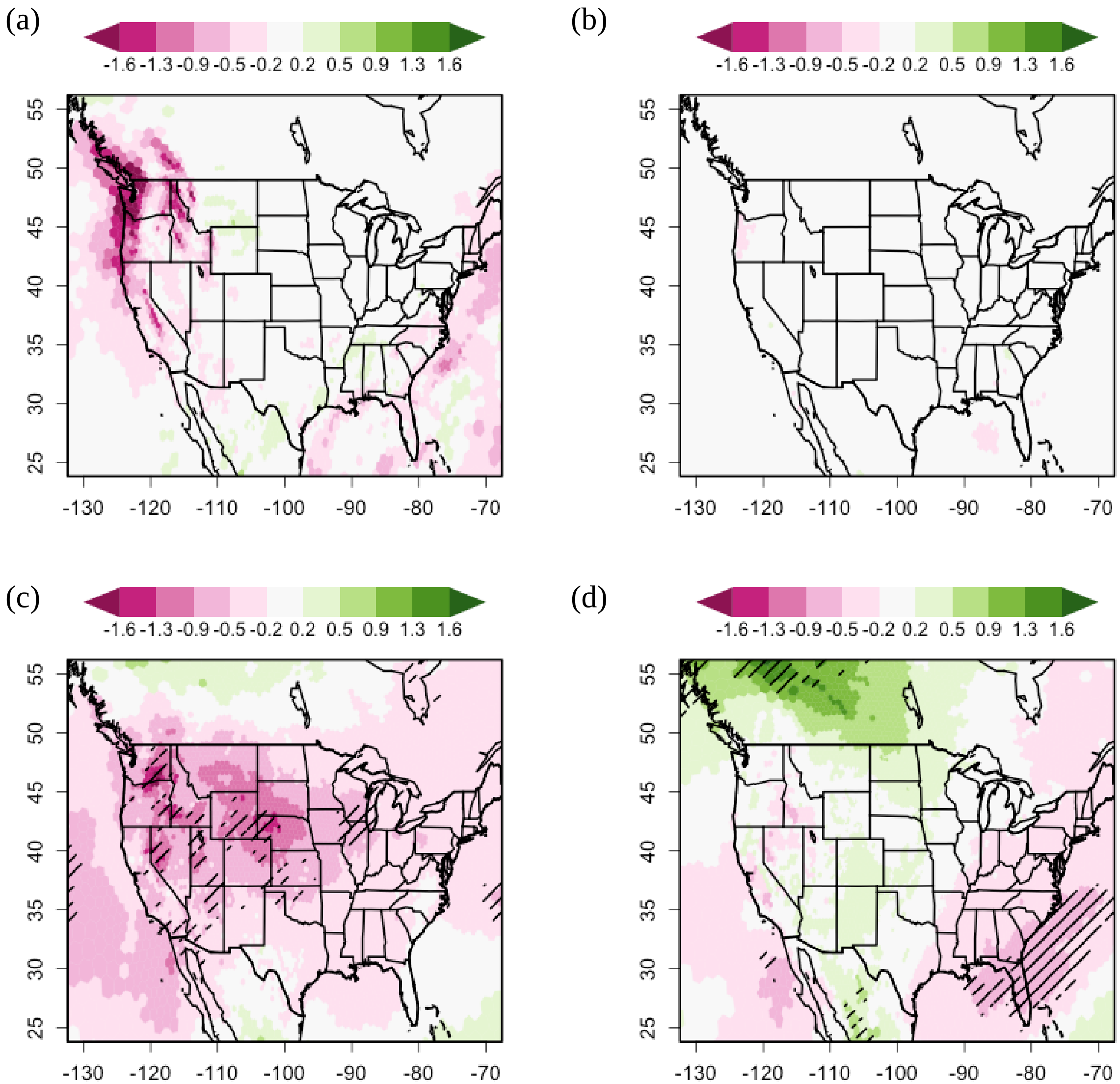

FIGURE 6: Impacts of deforestation on hyroclimatic variables. Panel a: change in moisture convergence (mm day^{-1}) in the FINE simulation pair. Panel b: change in evapotranspiration (mm day^{-1}) in the FINE simulation pair. Panel c: change in near-surface temperature (°C) in the FINE simulation pair. Panel d: change in near-surface temperature (°C) in the XFINE simulation pair. In panels c and d only, areas with statistically significant changes are hatched.

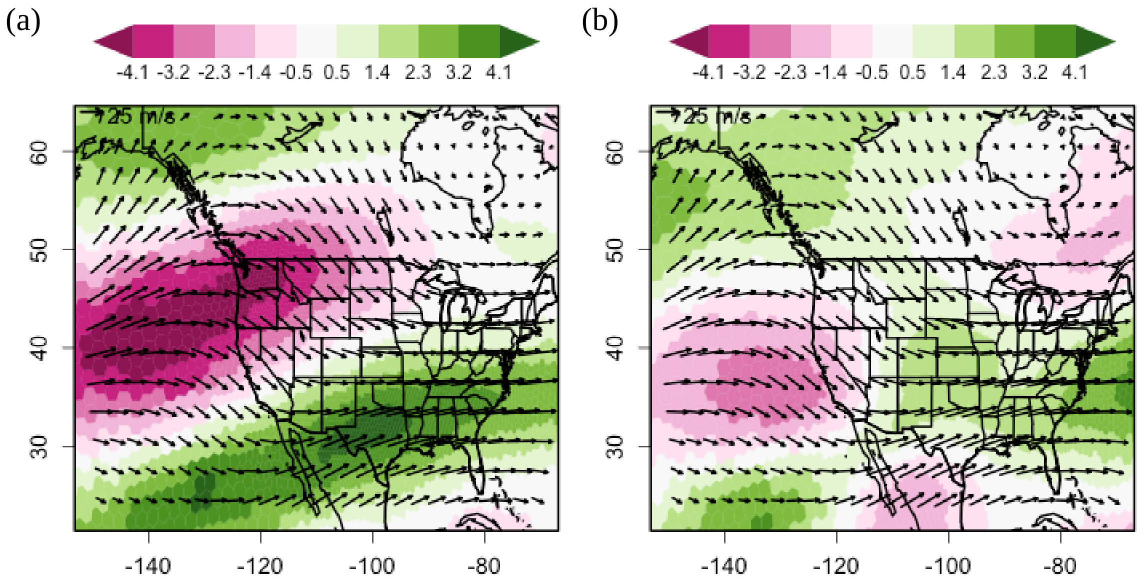

FIGURE 7: 250 hPa zonal wind and zonal wind anomalies over North America. The arrows show the zonal winds from FINE-FOR (panel a) and XFINE-FOR (panel b). Colors show the changes in 250 hPa zonal winds (m s^{-1}) resulting from deforestation from the FINE simulation pair (panel a) and the XFINE simulation pair (panel b).

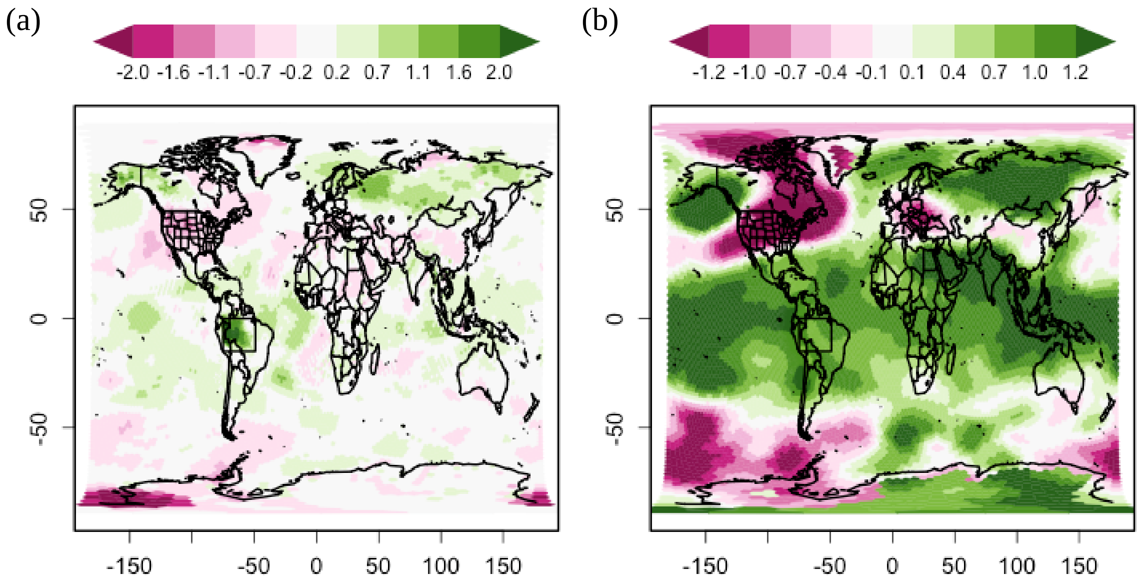

FIGURE 8: Changes in heating resulting from deforestation in the FINE simulation pair. Panel a: change in near-surface temperature (°C). The region of Amazon deforestation is boxed. Panel b: change in 850-300 hPa thickness (dam).

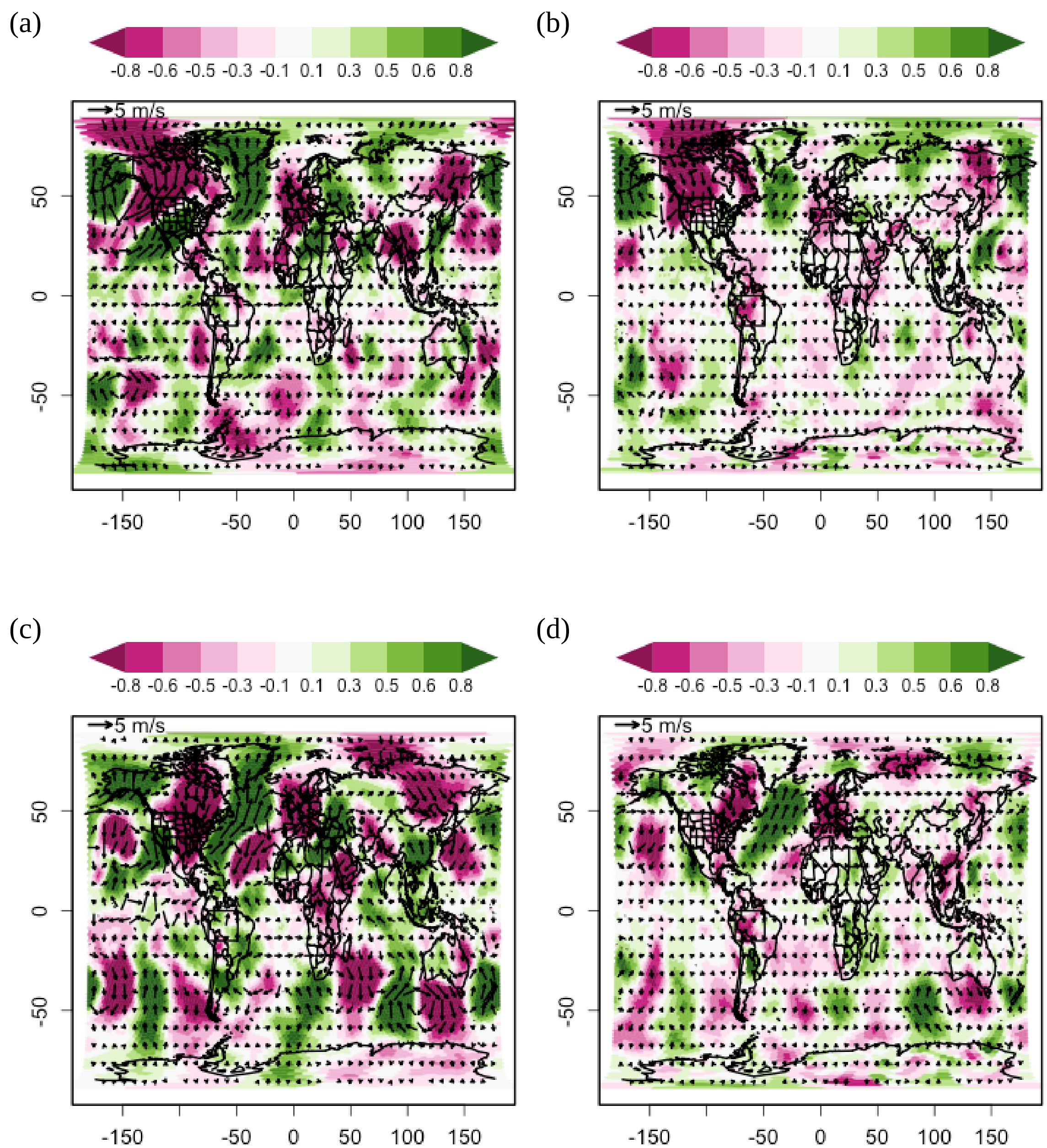

FIGURE 9: Deforestation-induced changes in the winds. The arrows show the changes in the wind vector and the colors show the changes in the meridional component of the wind (m s^{-1}). Panel a: changes at 250 hPa, FINE simulations. Panel b: changes at 850 hPa, FINE simulations. Panel c: changes at 250 hPa, XFINE simulations. Panel d: changes at 850 hPa, XFINE simulations.

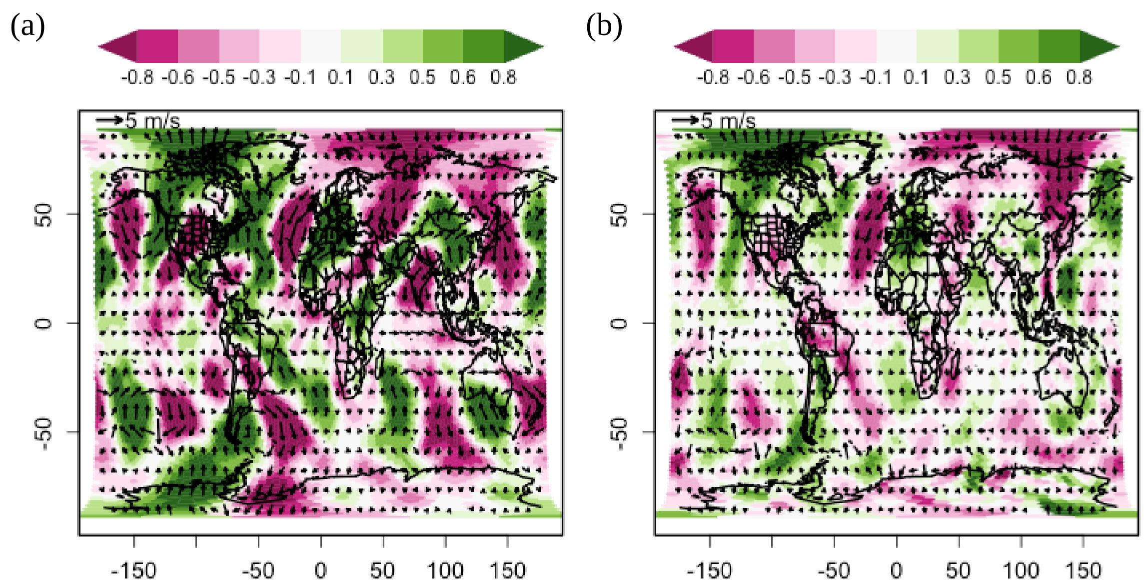

FIGURE 10: Deforestation-induced changes in the winds in the COARSE simulation pair. The arrows show the changes in the wind vector and the colors show the changes in the meridional component of the wind (m s^{-1}). Panel a: changes at 250 hPa. Panel b: changes at 850 hPa.